International Journal of GEOMATE, Dec., 2023 Vol.25, Issue 112, pp.83-90
ISSN: 2186-2982 (P), 2186-2990 (O), Japan, DOI: https://doi.org/10.21660/2023.112.g13177
Geotechnique, Construction Materials and Environment

MITIGATING SOIL COMPACTION IN SUGARCANE FIELDS: EXPERIMENTAL AND SIMULATION STUDY OF PLUNGER CONFIGURATIONS

Juthanee Phromjan[1,2,3], Michael Kaliske[2] and Chakrit Suvanjumrat[1,3*]

[1]Department of Mechanical Engineering, Faculty of Engineering, Mahidol University, Nakhon Pathom, 73170, Thailand;
[2]Institute for Structural Analysis, Technische Universität Dresden, Dresden, 01062, Germany;
[3]Laboratory of Computer Mechanics for Design (LCMD), Department of Mechanical Engineering, Faculty of Engineering, Mahidol University, Nakhon Pathom, 73170, Thailand

*Corresponding Author, Received: 27 May 2023, Revised: 27 Nov. 2023, Accepted: 30 Nov. 2023

ABSTRACT: The detrimental impact of soil compaction resulting from agricultural machinery remains a significant concern in contemporary agriculture, influencing crop growth and production costs. This research employs a combination of experimental and simulation methods to investigate various configurations of plungers, representing features of agricultural equipment. Conducted in a laboratory setting, the study focuses on sandy clay loam soil, pertinent to sugarcane fields in Thailand. The soil-structure interaction model for plungers is developed using the finite element method, incorporating a modified Cam-clay plasticity model based on the critical state concept, and porous elasticity for soil simulation. Different plunger shapes, each producing distinct effects, are meticulously detailed. The outcomes of this research serve as a practical guide for the future design and development of agricultural equipment, offering insights to mitigate soil compaction issues and enhance productivity. The straightforward environmental arrangement employed enhances the applicability of the findings to real-world agricultural settings.

Keywords: Agriculture, Finite element method, Soil compaction, Soil-structure interaction

1. INTRODUCTION

With the rise in population, the utilization of heavy-duty agricultural machinery, and the push for intensive cultivation to ramp up productivity, there's a growing need to reckon with the consequences on soil. This has led to soil compaction and hindered fluid infiltration due to altered physical and dynamic properties. The hefty external force exerted by these structures, especially from vehicle traffic and equipment, is a significant culprit, diminishing the number of soil pores. Consequently, these effects have a direct impact on the development of plant roots, resulting in a reduction in both the quality and quantity of agricultural production. It's crucial to assess the structural effects of these machines to understand how they contribute to soil stress distribution. This evaluation is pivotal for effective soil compaction management, which, in turn, can lead to improved soil quality and a more sustainable approach to agriculture.

Research has delved into the impact of tread patterns, tire size, and machinery on pressure distribution and soil compaction [1-3]. The topsoil, a crucial zone for crop field root development, exhibited significant responsiveness to applied pressure. The study also explored the influence of different equipment operations on stress transmission [4, 5], utilizing both field and laboratory testing for compacted soil examination. While field testing is valuable, laboratory testing stands out for its higher repeatability and more precise parameter control [6, 7].

The Finite Element Method (FEM), a simulation approach used in the lab, allows for the analysis of complex and nonlinear behaviors of agricultural machines. While FEM enables a virtual representation of these behaviors not directly observable through experimental or analytical methods, there remains a mystery regarding the effects of various machinery shapes during different operations. Current knowledge primarily addresses the impact of uniform ground pressure, leaving the intricacies of different machinery shapes in question [9-12]. Promjan and Suvanjumrat [13] proposed an integrated method using FEM and an empirical model to analyze non-pneumatic tire-soil compaction. Raguiara et al. [14] modeled soil compaction in a sugarcane crop through FEM. Hu et al. [15] modeled soil-tool interaction through the smoothed particle hydrodynamics (SPH) method. Swamy et al. [16] concluded the modeling techniques of tire-deformable soil interactions and their validations to confirm accuracy. Consequently, the machine's performance, particularly tire traction affecting energy consumption, demands focused attention. Therefore, a comprehensive understanding of the structural design influencing soil properties in the agricultural field becomes crucial to meet performance expectations.

2. RESEARCH SIGNIFICANCE

This research seeks to present insights into the impact of different configurations on soil compaction, specifically in a soil type suitable for crop fields. A robust numerical method, the FEM, was employed, with particular emphasis on the significance of the Modified Cam-clay (MCC) plasticity model within the FEM framework. To gather essential material properties of the sampled soil, laboratory testing was conducted. Subsequently, the finite element models were meticulously compared to experimental data to ascertain reliability. The validated model was then employed to discuss the effects of various configurations. The findings of this study hold the potential as valuable guidance for the design and advancement of agricultural equipment or tire tread patterns in future endeavors.

3. MATERIALS AND METHODS

The soil used for testing was collected from a sugarcane field located in Nakhon Pathom province, Thailand, known for its high sugarcane productivity. Initially, sieve and hydrometer testing procedures were employed to analyze the soil composition. The sampled soil was identified as sandy clay loam (SCL), with silt, sand, and clay constituting 13%, 64%, and 23%, respectively. This particular soil type is well-suited for crop fields, especially for cultivating sugarcane [5, 17, 18]. The initial conditions for testing included a soil dry bulk density (BD) of 1.5 Mg/m³ and a soil moisture content of 15% w/w. These values fall within the suitable range for optimal crop growth [19].

3.1 Soil Consolidation

The Oedometer test, as shown in Fig. 1(a), is carried out to quantify soil consolidation. The soil samples, measuring 6.35 cm in diameter and 2.00 cm in height, undergo this testing procedure. The compression ratio (C_C) and recompression ratio (C_R) can be determined. Subsequently, key parameters are derived from the results, including the compression index (λ) and swelling index (κ), calculated as follows:

$$\lambda = C_C / \ln(10) \tag{1}$$

$$\kappa = C_R / \ln(10) \tag{2}$$

Moreover, the Oedometer test allows for the evaluation of pre-consolidation pressure (P_c) and initial void ratio (e_0). These metrics are pivotal in comprehending the soil's behavior and its response to applied stress, furnishing valuable insights for subsequent analyses and engineering assessments.

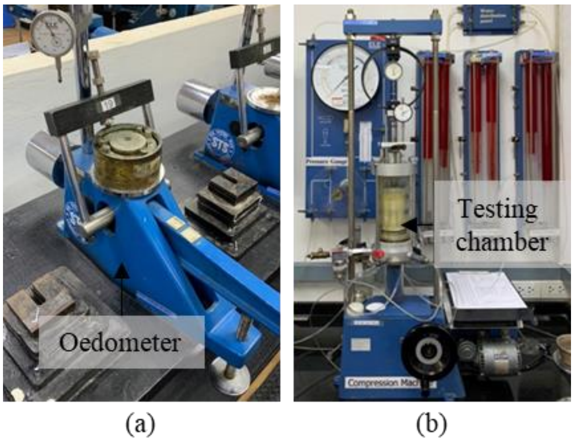

Fig.1 (a) The Oedometer test and (b) triaxial test

3.2 Triaxial Test

The isotropically consolidated undrained (CU) test, depicted in Fig. 1(b), is a triaxial shear test aimed at determining the elastoplastic parameters of soil samples for the MCC model, with a focus on the critical state stress ratio (M_C). Additionally, if the mean shearing stress along the straight line corresponding to the failure point under each confining pressure is negative, its absolute value is defined as the elastic limit of the tensile strength (p_t^{el}) [20].

In this test, three varying confining pressures (100, 200, and 300 kPa) were applied in the pressure chamber. For axial compression tests, the confining pressure was kept constant while applying axial load until material failure or a rapid change in strain occurred without significant stress variation. A very slow strain rate of 2.5% per hour was employed to minimize the retardation time effect. The soil specimen dimensions for this test were a height and diameter of 9.70 and 4.8 cm, respectively. Vertical displacement and principal effective compressive stress (σ_i) of soil specimens were recorded during the tests.

Equations (3) and (4) are employed to calculate the deviatoric stress (q) and mean principal stress (p) based on the collected data. These tests and parameters contribute to a comprehensive understanding of the soil's mechanical behavior and aid in establishing critical values for modeling purposes and geotechnical engineering analyses.

$$q = \sigma_1 - \sigma_3 \tag{3}$$

$$p = (\sigma_1 + \sigma_2 + \sigma_3) / 3 \tag{4}$$

while the $\sigma_2 = \sigma_3$ is assumed according to testing conditions.

3.3 Plunger Test

A cylindrical plunger with a diameter of 10 cm was employed as the testing device for the plunger test. This plunger was integrated into the universal testing machine (QC-506, ComeTech) and applied to the sampled soil within a wooden box, as illustrated in Fig. 2. The dimensions of the box were 300×300×200 mm (W×L×H), strategically chosen to mitigate any wall effects, in line with recommendations from Onwualu and Watts [21]. The plunger was systematically moved downward with a strain rate of 2.5% per hour, carefully chosen to minimize the impact of retardation time. Vertical displacement ranged from 5 to 25 mm, with 5 mm intervals.

The sampled soil, with a controlled moisture content and density of 15% and 1.5 Mg/m^3 respectively, was gradually filled into the box layer by layer. Each test involved newly prepared soil. Compression force and vertical displacement data were collected during testing. Additionally, the final soil surface deformation was captured using a handheld 3-dimensional (3-D) scanner. The soil bulk density of the soil sinkage was investigated by collecting soil samples using a known volume soil core, subsequently dried at 105°C in an oven for over 24 hours. The dried soil was weighed with a precision digital scale (UX-620H, Shimadzu). The resulting soil bulk densities are detailed in Table 1, revealing an observable trend of increased soil bulk density with the escalation of soil deformation. Additionally,

Fig.2 Plunger test

Table 1 Soil bulk density evaluation

Soil deformation (mm)	Soil bulk density (Mg/m^3)
5	1.960
10	1.976
15	1.979
20	1.965
25	2.026

the trend of the results remained consistent with the experimental findings on a larger scale, as proposed in previous works [3, 4].

3.4 Finite Element Analysis

The MCC plasticity model, integrating the critical state concept with porous elasticity, was employed to simulate the impact of voids on the elastic behavior of the soil model. This model stands out as one of the most extensively utilized material models in geotechnical applications. The MCC model incorporates an associated flow rule, ensuring that the flow potential aligns with the yield function, and plastic flow occurs normally to the yield surface as a function of principal stress and modified stress invariant [22, 23]. This approach is articulated by the following equation:

$$f_{cc} = \frac{1}{\beta^2}\left(\frac{p}{a_h} - 1\right)^2 + \left(\frac{t}{M_C a_h}\right)^2 - 1 \quad (5)$$

where t denotes a modified stress invariant and β and a_h denote material parameters.

In the absence of cohesion and considering no yield in tensile stress states, β was defined to be equal to 1. Simultaneously, when the flow stress in triaxial tension equals the flow stress in triaxial compression, t is equated to q. The rewritten form of the yield surface is expressed as follows [23]:

$$f(p,q) = \left(\frac{p}{a_h} - 1\right)^2 + \left(\frac{q}{M_c a_h}\right)^2 - 1 = 0 \quad (6)$$

The influence of voids on the elastic properties of the soil model can be explored. The alteration in void ratio is directly proportional to the change in logarithmic pressure during elastic loading. Furthermore, in cases where the material possesses a non-zero elastic tensile strength, it can be expressed as follows:

$$de^{el} = -\kappa d\left(\ln\left(p + p_t^{el}\right)\right) \quad (7)$$

Conversely, λ represents a variable assuming a linear relationship between the void ratio and the natural logarithm of the pressure during plastic loading, and it can be expressed as follows:

$$de^{pl} = -\lambda d\left(\ln p\right) \quad (8)$$

The finite element model of the soil triaxial test specimen was constructed in accordance with the experimental setup. The applied boundary conditions for the specimen model are illustrated in Fig. 3.

The cylindrical plunger, represented as a simple shape in the finite element analysis (FEA), is depicted in Fig. 4. It was meshed using hexahedron elements, totaling 1,520 elements. The soil model underwent a similar hexahedron element meshing approach, with the top layer featuring finer elements to facilitate a detailed investigation of soil sinkage. The entire soil model comprised a total of 138,240 elements. Validated soil properties obtained from the FEA of the soil triaxial test were assigned to the soil model. The entire soil model was considered a homogeneous material, with constant parameters throughout the analysis. However, it's essential to acknowledge that significant variations between measurement and simulation results might arise due to factors like soil moisture [24].

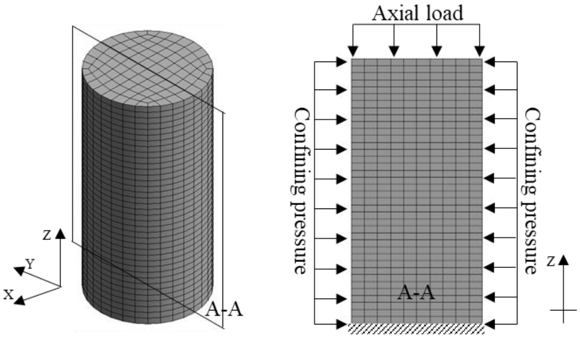

Fig.3 Finite element model of the triaxial test

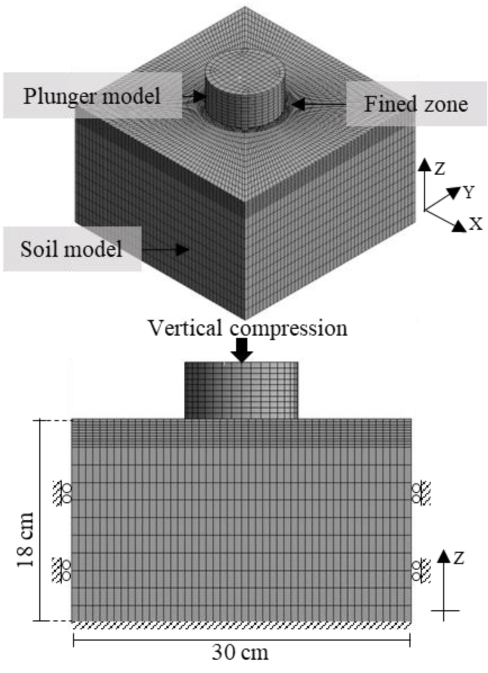

Fig.4 Finite element model of the cylinder plunger-soil compression

To simulate the interaction between the topsoil surface and the plunger, a contact algorithm was employed, with the topsoil surface assigned to make contact with the bottom and side surfaces of the plunger. Vertical displacement was applied to the plunger, compressing the soil surface, with variations from 5 to 25 mm at intervals of 5 mm.

All finite element models were executed using ANSYS software on a personal computer equipped with a core i5 CPU and 32GB of RAM.

4. RESULTS AND DISCUSSION

4.1 Triaxial Test

The constitutive model features an ellipsoidal yield surface within the stress space. The critical state is defined by the intersection of the yield surface with a line of slope M_C. In this case, Poisson's ratio (ν) was reasonably assumed. Given the absence of cohesion and the exclusion of tensile stress states within the yield surface, the parameter β was set to 1. The soil properties obtained from testing are succinctly summarized in Table 2.

Figure 5 illustrates the comparison of results, showcasing a strong agreement between the FEA results and the experimental results across all three confining pressures. The finite element model exhibited an average R^2 value of 0.957, indicating a high level of correlation between the simulated and experimental outcomes.

Table 2 Soil properties

Parameters	Value, Unit
MCC	
Compression index, λ	0.0866
Slope of critical state line, M_C	0.94
Preconsolidation pressure, P_c	13.73, kPa
Porous Elasticity	
Swell index, κ	0.0353
Elastic limit of tensile strength, p_t^{el}	31.92, kPa
Poisson's ratio, ν	0.2
Initial void ratio, e_0	0.765

4.2 Plunger Test

The results of the cylindrical plunger test are presented in the compression vs. deformation graphs, as depicted in Fig. 6. The discernible difference in slope between the experimental and FEA approaches reflects the challenge mentioned earlier. In practical terms, as soil undergoes compression under a specific pressure or experiences a reduction in moisture content, its strength tends to increase [9, 25], manifesting in a steeper slope in the experimental results. Conversely, the FEM struggles to fully capture all aspects of soil behavior, resulting in a lower slope in the FEA results. Despite this limitation, the FEM proves adequate in describing small deformations of the soil.

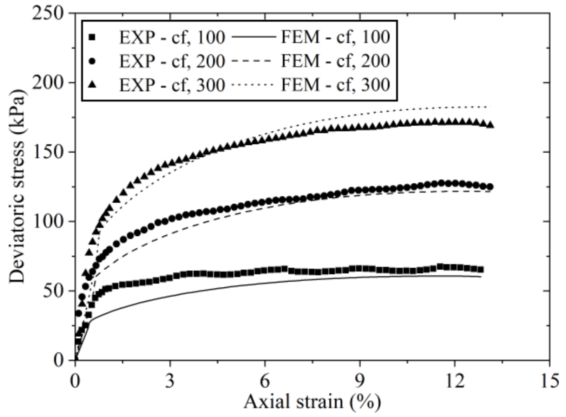

Fig.5 Comparison of the triaxial test results between the finite element method and experiment

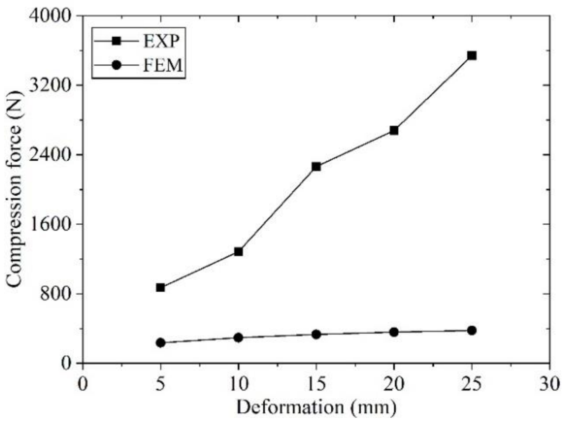

Fig.6 Force vs. deformation graphs of the cylindrical plunger test by finite element method and experiment

However, the analysis results can undergo further examination. Initially, both the experimental and FEA results are presented in the context of a mathematical model, which was scrutinized using a linear regression approach as follows:

$$F_{C,EXP} = 134.75D + 106.08 \tag{9}$$

$$F_{C,\mathrm{FEA}} = 7.031D + 214.11 \tag{10}$$

where $F_{C,EXP}$, $F_{C,\mathrm{FEA}}$ denote the compression force of experiment and FEA, respectively, and D denotes a vertical deformation. The R^2 of each equation is equal to 0.984 and 0.950, respectively.

It is noticeable that the slope of the experimental result exceeded that of the FEA result by a factor of 19.17. By multiplying the slope of the FEA result by 19.17, the $F_{C,\mathrm{FEA}}$ model can be reformulated as follows:

$$F_{C,\mathrm{FEA}} = (7.031 \times 19.17)D + 214.11 \tag{11}$$

The predicted compression force, calculated using Eq. (11), exhibited consistency with the experimental results, showing an average error of 6.66%. Hence,

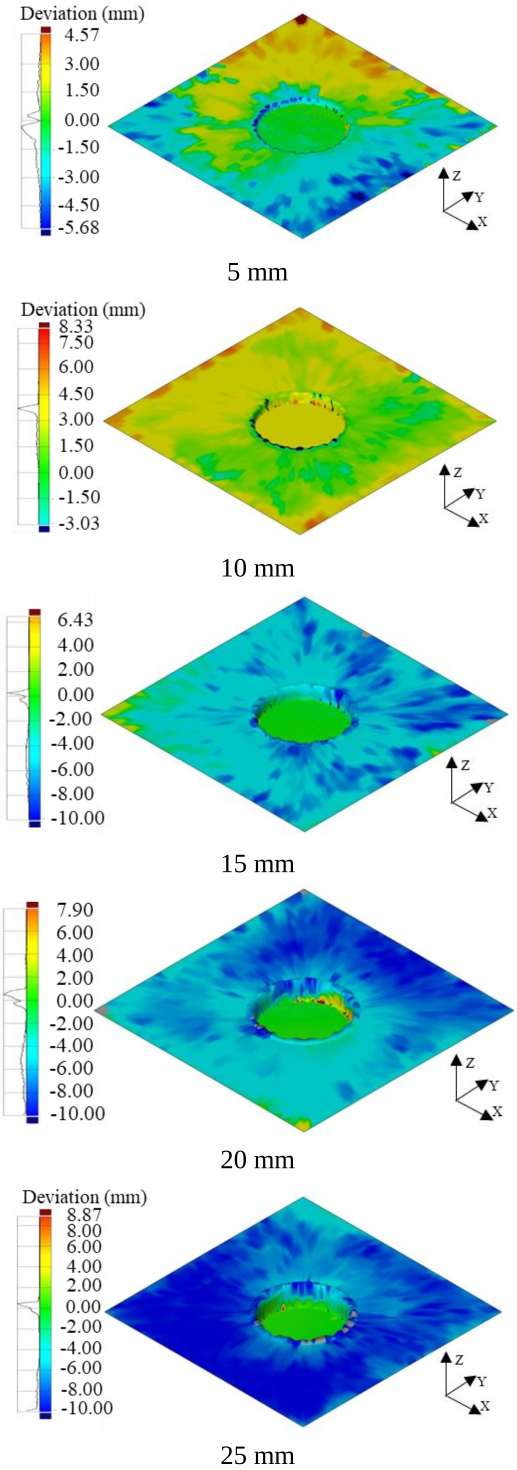

Fig.7 Comparison results of soil surface deformations

the finite element (FE) model of the cylindrical plunger test, along with the modified model, can be employed for the comprehensive study of soil-structure interaction.

The comparison of soil surface deformations under different compression depths between the FEM and experimental results is depicted in Fig. 7. The experimental surfaces were obtained using a 3-D scanner, while the simulation surface was collected from nodes at the top surface of the soil model. The color contour illustrates the deviations between the soil surfaces. High error was observed at the side wall of the cylindrical sinkage, particularly increasing with displacement due to prolonged compression times leading to soil moisture reduction. This behavior, related to soil shrinkage, was not accurately captured by the developed soil model. However, the model proves effective in predicting soil deformation for experiments with smaller depths. Notably, the circular surface of the cylindrical sinkage demonstrated high accuracy. Despite limitations in capturing specific behaviors, the FEM remains a valuable tool for studying the effects of configuration on soil deformation related to soil compaction, particularly in scenarios involving smaller depths and circular surfaces.

4.3 Plunger Configuration Effects

The FEM was employed to simulate basic configurations of a plunger in the plunger test, facilitating a parametric study for various factors with easier boundary control and reduced analysis resources. Three commonly used shapes for agricultural equipment—a half-sphere, square, and cylinder—were simulated. The diameter of the half-sphere and cylinder plungers was set at 10 cm, matching the size of the square plunger. This configuration aimed to explore the effects of different shapes of agricultural equipment with the same size, potentially influencing pressure distribution on the soil and, consequently, soil compaction.

All three plunger shapes were pressed onto the soil surface with a vertical compression force of 200 N, maintaining the same boundary conditions as the cylinder plunger test illustrated in Fig. 4. However, there was a slight difference in the meshing of the soil model for the square plunger case, where a fine contact zone was created according to the plunger shape while maintaining the same element size. Despite the varied plunger shapes, the average size of the elements remained similar. The material properties of all plungers were set as steel.

Simulation results, presented in Fig. 8, indicated the highest vertical deformation in the half-sphere case, significantly greater than in the other cases. Excessive vertical soil deformation not only hinders tire or equipment movement but can also be detrimental in agricultural applications. Conversely, the square-shaped plunger exhibited the minimum deformation. The trend of results aligned with the contact area of the plunger, directly influencing contact pressure and penetration.

The color contour of stress revealed that the minimum stress occurred in the square case, which had the largest contact area. This suggests lower soil compaction, promoting greater compression energy dissipation [2]. Additionally, the larger contact area induced higher drawbar pull, beneficial for agricultural applications typically performed on soft ground [26].

The simulation results also highlighted the importance of accounting for concentrated stress at the corners of the structure in equipment design. This stress concentration occurs in a small area but at a high value, potentially serving as the source of soil collapse or excessive soil compaction. Furthermore, the horizontal extent of the compression effects induced by the plunger was particularly severe for the round structure. This underscores the need for careful consideration of stress distribution and its spatial extent in designing agricultural equipment to mitigate adverse effects on soil structure and compaction.

5. CONCLUSION

The FEM incorporating a plasticity model and porous elasticity demonstrated its effectiveness in capturing soil deformation under pressure. Additionally, it provided detailed insights into nonlinear behaviors such as pressure distribution and stress concentration. The research findings underscored the substantial impact of soil moisture content on soil strength. Different configurations with equivalent sizes exhibited significant variations in soil compaction due to distinct applied pressures. This emphasizes the importance of considering soil moisture content in soil compaction management and suggests that designing agricultural equipment can play a crucial role in this regard. The research procedures are slated to be extended for a larger scale of soil-structure interaction analysis in the near future, further enhancing our understanding of these complex interactions.

6. ACKNOWLEDGMENTS

This research received financial support from the Thailand Science Research and Innovation (TSRI) and the National Research Council of Thailand (NRCT) under the Royal Golden Jubilee Ph.D. Program (Grant No. PHD/0049/2561).

7. REFERENCES

[1] Barbosa A. P., and Magalhaes S. G., Tire tread pattern design trigger on the stress distribution over rigid surfaces and soil compaction, Journal of Terramechanics, Vol. 58, 2015, pp. 27-38.

[2] da Silva R. B., Iori P., de Souza Z. M., Pereira D. de M. G., Vischi Filho O. J., and de M Silva F. A., Contact pressures and the impact of farm equipment on Latosol with the presence and absence of sugarcane straw. Ciência e

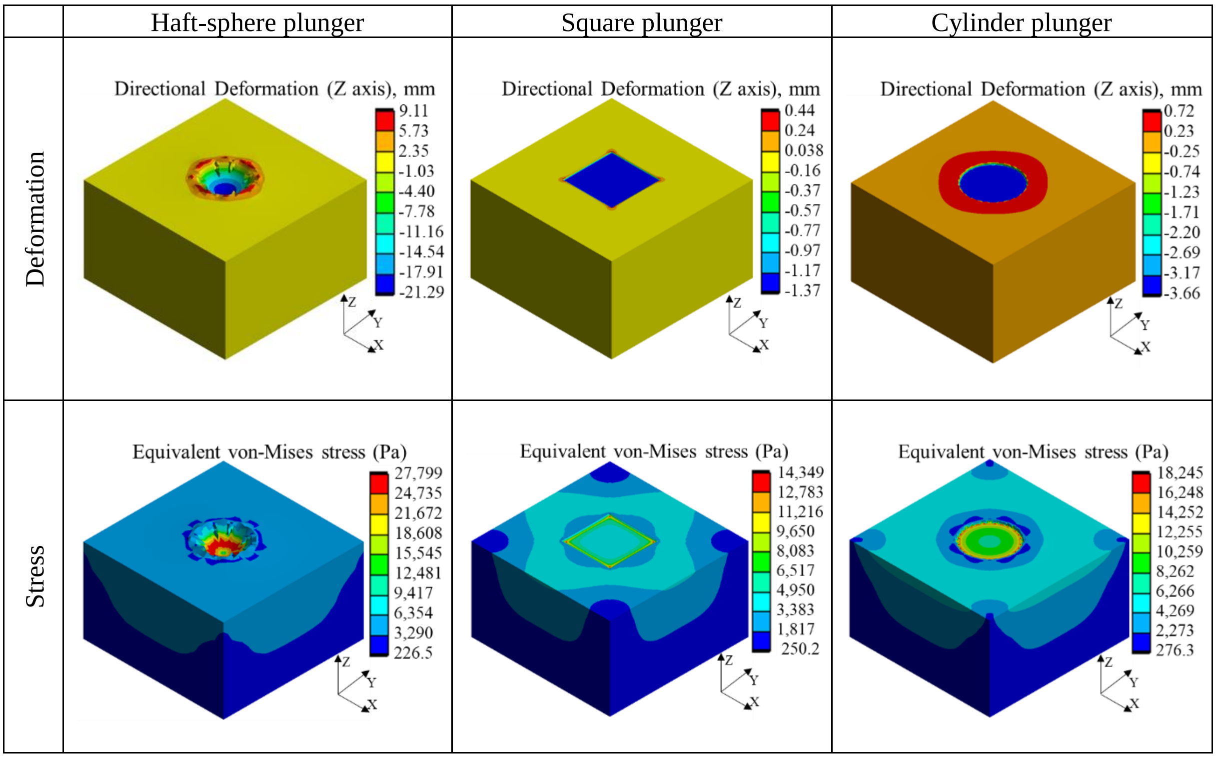

Fig.8 Deformation and stress results of soil by various types of plunger compression

Agrotecnologia, Vol. 40, Issue 3, 2016, pp. 265-278.

[3] Phakdee S., and Suvanjumrat C., Development of a tire testing machine for evaluating the performance of tractor tires based on the soil compaction, Journal of Terramechanics, Vol. 110, 2023, pp. 13-25.

[4] Wellingthon da Silva G. J., Etienne D., Isabella C. De M., Cezar F. A. J., Camila V. V. F., and Zigomar M. de S., Prediction of soil stresses and compaction due to agricultural machines in sugarcane cultivation systems with and without crop rotation, Science of The Total Environment, Vol. 681, 2019, pp. 424-434.

[5] Guilherme A.F. Castioni, Renato P. de Lima, Maurício R. Cherubin, Ricardo O. Bordonal, Mario M. Rolim, and João L.N. Carvalho, Machinery traffic in sugarcane straw removal operation: Stress transmitted and soil compaction, Soil and Tillage Research, Vol. 213, 2021, 105122.

[6] Ansorge D., and Godwin R. J., The effect of tyres and a rubber track at high axle loads on soil compaction, Part 1: Single axle-studies, Biosystems Engineering, Vol. 98, 2007, pp. 115-126.

[7] Mohamed M. A., Elhussieny S., Emam M. A., and Elhafiz M. M. A., Tire-soil interaction simulation using finite element method to investigate their deformation and sinkage. SAE Technical Paper Series. 2023.

[8] Omar G. C., Ciro E. I. C., Carlos A. R. M., Guillermo U. S., Luís H Hernández G., Guillermo U. C., and Miguel H. S., Three dimensional finite element model of soil compaction caused by agricultural tire traffic, Computers and Electronics in Agriculture, Vol. 99, 2013, pp. 146-152.

[9] Payam F., Abdollah G., Ahmad S. M., and Gholamhossein S., Finite element modeling of the interaction of a treaded tire with clay-loam soil, Computers and Electronics in Agriculture, Vol. 162, 2019, pp. 793-806.

[10] Suvanjumrat C., and Phromjan J., The contact patch characterization of various solid tire testing methods by finite element analysis and experiment, International Journal of GEOMATE, Vol. 19, 2020, pp. 25-32.

[11] Phromjan J., and Suvanjumrat C., Effects on spoke structure of non-pneumatic tires by finite element analysis, International Journal of Automotive Technology, Vol. 23, 2022, pp. 1437-1450.

[12] Phromjan J., and Suvanjumrat C., Development of solid tire model for finite element analysis of compressive loading, Songklanakarin Journal of Science and Technology, Vol. 43, Issue 1, 2021,

pp. 229-236.

[13] Phromjan J., and Suvanjumrat C., Non-pneumatic tire with curved isolated spokes for agricultural machinery in agricultural fields: Empirical and numerical study, Heliyon, Vol. 9, 2023, pp. e18984.

[14] Raguiara P. S., Mário M. R., Igor F. G., Elvira M. R. P., Uilka E. T., and Alexandre N. S., Numerical modeling of soil compaction in a sugarcane crop using the finite element method, Soil & Tillage Research, Vol. 181, 2018, pp. 1-10.

[15] Hu M., Gao T., Dong X., Tan Q., Yi C., Wu F., and Bao A., Simulation of soil-tool interaction using smoothed particle hydrodynamics (SPH), Soil & Tillage Research, Vol. 229, 2023, pp. 105671.

[16] Swamy V. S., Pandit R., Yerro A., Sandu C., Rizzo D. M., Sebeck K., and Gorsich D., Review of modeling and validation techniques for tire-deformable soil interactions, Journal of Terramechanics, Vol. 109, 2023, pp. 73-92.

[17] Esteban D. A. A., Souza Z. M., Tormena C. A., Lovera L. H., Souza Lima E., and Oliveira I. N., Soil compaction, root system and productivity of sugarcane under different row spacing and controlled traffic at harvest. Soil and Tillage Research, Vol. 187, 2019, pp. 60-71.

[18] Jimenez K. J., Rolim M. M., Gomes I. F., Lima R. P., Berrio L. L. A., and Ortiz P. F. S., Numerical analysis applied to the study of soil stress and compaction due to mechanized sugarcane harvest. Soil and Tillage Research, Vol. 206, 2021, 104847.

[19] Mukhopadhyay S., Masto R. E., Tripathi R. C., and Srivastava N. K., Chapter 14 – Application of Soil Quality Indicators for the Phytorestoration of Mine Spoil Dumps, in: Phytomanagement of Polluted Sites. Elsevier, Amsterdam, Netherlands, 2019, pp. 361-388.

[20] Xu X., Wang B., Fan C., and Zhang W., Strength and deformation characteristics of silty clay under frozen and unfrozen states, Cold Regions Science and Technology, Vol. 172, 2020, 102982.

[21] Onwualu A. P., and Watts K. C., Development of soil bin test facility. American Society of Agricultural Engineers, Vol. 13, 1989, pp. 89-1106.

[22] Roscoe K. H., and Burland J. B., On the generalized stress-strain behaviour of 'wet' clay, Engineering Plasticity, Vol. 169, 1968, pp. 535-609.

[23] Ansys® Mechanical, Release 2023 R1, Help System, Material Reference, ANSYS, Inc.

[24] Diarra H., Mazel V., Busignies V., and Tchoreloff P., Comparative study between Drucker-Prager/Cap and modified Cam-Clay models for the numerical simulation of die compaction of pharmaceutical powders, Vol. 320, 2017, pp. 530-539.

[25] Hamza M. A., and Anderson W. K., Soil compaction in cropping systems A review of the nature, causes and possible solution, Soil and Tillage Research, Vol. 82, 2005, pp. 121-145.

[26] Battiato A., and Diserens E., Tractor traction performance simulation on differently textured soils and validation: A basic study to make traction and energy requirements accessible to the practice, Soil and Tillage Research, Vol. 166, 2017, pp. 18-32.